PRAMANA
— journal of
physics

Vol. 56, No. 1
January 2001
pp. 87–94

Overlapping $B^3\Pi_{0u} \leftarrow X^1\Sigma_g^+$ and $^1\Pi_{1u} \leftarrow X^1\Sigma_g^+$ non-radiative characteristic of Br_2 vapour in the wavelength region 505–541 nm

RAMESH C SHARMA and S N THAKUR*
Physics Department and Centre for Laser Technology, Indian Institute of Technology, Kanpur 208 016, India
*Laser Spectroscopy Laboratory, Banaras Hindu University, Varanasi 221 005, India

MS received 24 May 1999; revised 13 September 2000

Abstract. The vibronic vapour phase photoacoustic spectrum of Br_2 in the wavelength region 505–541 nm (19796–18480 cm^{-1}) has been recorded using microphone as well as pump-probe method. Discrete vibronic bands superimposed on a monotonically increasing continuum background towards the dissociation limit results from the overlapping $B^3\Pi_{0u}^+ \leftarrow X^1\Sigma_g^+$ and $^1\Pi_{1u} \leftarrow X^1\Sigma_g^+$ electronic transitions. Vibronic bands originating from $v'' = 0$ have been used to estimate the relative rate of non-radiative relaxation as a function of the excited state $B\,^3\Pi_{0u}$ vibrational quantum number v'. A comparison with the optical absorption spectroscopy of Br_2 leads to the identification of three broad spectral regions between 505 and 541 nm (19796 and 18480 cm^{-1}) on the basis of different non-radiative relaxation processes.

Keywords. Photoacoustic spectrum; laser spectroscopy; non-radiative channels; predissociation effects.

PACS Nos 42.60; 52.80

1. Introduction

The Br_2 vapour has been the subject of several high resolution spectroscopic studies on the $B^3\Pi_{0u}^+ \leftarrow X^1\Sigma_g^+$ system and the rotational fine structure as well as the intensity distribution in the vibronic bands have been well understood through the research work of Coxon [1], Horsely and Barrow [2], Barrow *et al* [3], and Coxon [4]. The continuum extending to the lower wavelengths from the dissociation limit of the $B\,^3\Pi_{0u}^+ \leftarrow X^1\Sigma_g^+$ transition has been studied by Le Roy *et al* [5] who estimated the intensity contributions to the continuum resulting from the $^1\Pi_{1u} \leftarrow X^1\Sigma_g^+$ and $B^3\Pi_{0u}^+ \leftarrow X^1\Sigma_g^+$ transitions in the wavelength range 320–500 nm (31241–19994 cm^{-1}). Time dependent photoacoustic spectrum of Br_2 was first obtained by Koseki *et al* [6] using the only 532 nm radiation from Q-switched Nd-YAG laser.

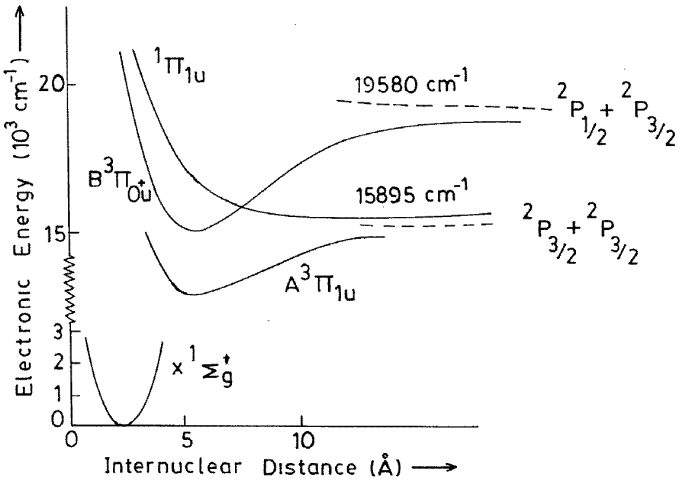

Figure 1. Partial potential energy diagram of Br_2 molecule.

In the present work we have estimated the relative non-radiative relaxations of excited molecules in $B^3\Pi_{0u}^+$ and $^1\Pi_{1u}$ states from the analysis of vibronically resolved photoacoustic spectrum of Br_2 vapour in the wavelength range 505–541 nm (19796–18480 cm^{-1}) for the first time. The spectral features of Br_2 vapour in this frequency range can be understood with the help of the partial potential energy diagram given in figure 1.

2. Experimental

The third harmonic (355 nm) radiation from a Nd-YAG laser [(Spectra Physics, Model DCR-III) Pumped Dye Laser] (Spectra Physics, Model PDL-2) in the yellow–green region using C-500 dye solution in methanol. The output energy of the dye laser was 4–7 mJ/pulse with a bandwidth of 0.05 nm and pulse repetition rate of 10 Hz.

The sample cell containing Br_2 vapour was made from a Pyrex glass tube 15 cm in length and 4.6 cm in diameter. Quartz windows were fitted at the two ends and the two separate needle valves connected the photoacoustic cell. One needle valve was for the sample reservoir which could be maintained at liquid N_2 temperature and at room temperature and other needle valve connected it to the vacuum pump. The excitation from dye laser was made collinear with the probe beam from a 2 mW He–Ne laser and the latter was directed to the pin hole photodiode [EG&G Model-9025] detector assembly by means of mirrors schematically shown in figure 2. The absorption of the dye laser beam by the sample creates a concave lens-like thermal refractive index gradient in the cell that makes the probe laser beam diverge. The intensity variation of the probe beam at the detector leads to the electric signal as the dye laser wavelengths are varied, and fed into a box-car averager [EG&G model 162] with gated integrator [model 166].

Initial experiments in Br_2 vapour were also carried out with the tunable dye laser and a photoacoustic cell identical to the one described above but fitted with a microphone. It was

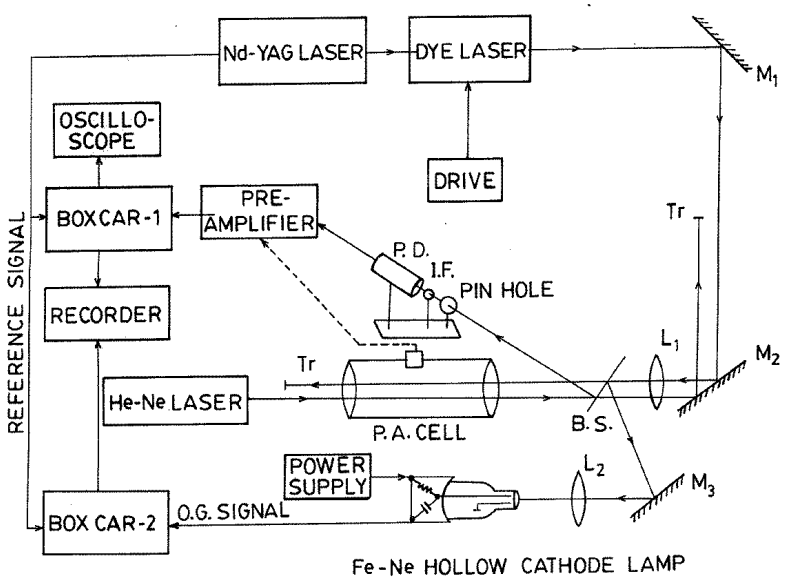

Figure 2. Schematic diagram of photoacoustic and photothermal experimental setup.

found that Br_2 vapour damaged the microphone so that it could not be used for more than two hours in the presence of the vapour. Vapour pressure of Br_2 was 285 Torr. All results reported here were obtained by using the photothermal detection method using He–Ne probe laser.

When recording the spectrum the output of the box-car averager is fed to the first pen of a two pen chart recorder. The other pen of the chart recorder is connected to the optogalvanic signal resulting from a Fe–Ne hollow cathode lamp that is illuminated by a small fraction of the tunable dye laser radiation for the purpose of wavelength calibration. The experimental setup is schematically shown in figure 2.

3. The photoacoustic spectrum of $B^3\Pi_{0u}^+ \leftarrow X^1\Sigma_g^+$ system

The photoacoustic spectra of Br_2 vapour, recorded as described above, were normalized by dividing the photoacoustic signal at each wavelength by the corresponding relative output power of the tunable dye laser. The normalized spectrum shown in figure 3a exhibits a banded structure superimposed on a background continuum that increases towards shorter wavelengths, rather sharply in the frequency range 19579–18480 cm^{-1}, and then relatively slowly to still higher frequencies. The discrete bands exhibit increasing contrast in going from the lower to the higher frequency which reaches a maximum somewhere on the plateau region and then decreases to zero in the region of the dissociation limit of the $B^3\Pi_{0u}^+$ state (see figure 3a).

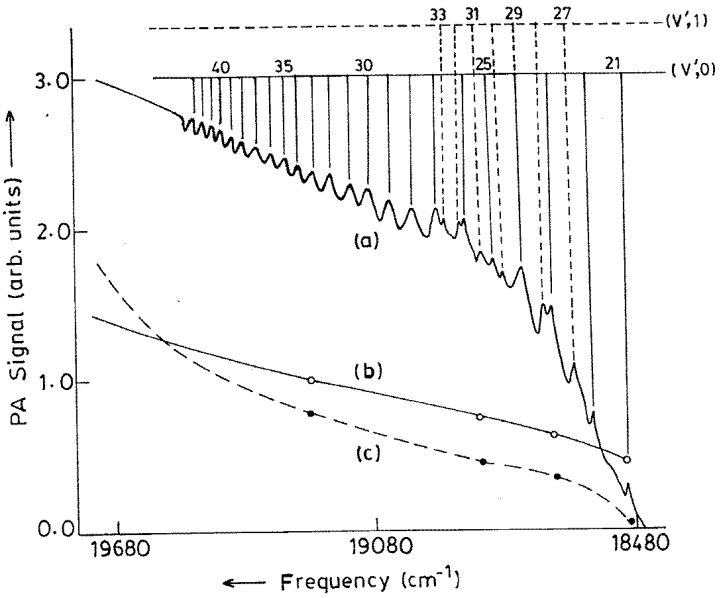

Figure 3. Normalized photoacoustic spectrum of Br_2 vapour (**a**), relative absorption strength of $B^3\Pi^+_{0u} \leftarrow X^1\Sigma^+_g$ (**b**), and relative absorption strength of $^1\Pi \leftarrow X^1\Sigma^+_g$ (**c**).

4. Analysis of the photoacoustic spectrum

The discrete vibronic bands in the photoacoustic spectrum are easily identified in the light of the vibrational analysis of the corresponding optical spectrum by Coxon [4]. The natural abundance of ^{79}Br is almost equal to that of ^{81}Br and hence the proportion of $^{79}Br_2$, $^{81}Br_2$ and ^{79}Br ^{81}Br in the bromine vapour would be in the ratio of 1:1:2. It has not been possible to observe isotropic splitting in the vibronic bands of photoacoustic spectra and therefore our discussions are based on the assumption that measured peak position as well as the peak intensities correspond to the ^{79}Br ^{81}Br isotope species in view of its higher abundance. The isotopic spectral peaks belonging to $^{79}Br_2$ and $^{81}Br_2$ would lie on either side of the ^{79}Br ^{81}Br peak and would lead to a symmetric distortion of the vibronic band profile of the most abundant isotropic species. It is found that main progressions involve $v'' = 0, 1$. Photoacoustic signal intensity $I_{\rm PA}$, in a pulsed excitation can be written as

$$I_{\rm PA} = I_{\rm OA} A_{\rm nr} h\nu, \tag{1}$$

where $I_{\rm OA}$ is optical absorption intensity calculated as the product of Frank–Condon factor and the corresponding Boltzmann factor $\exp(-\Delta Ev''/KT)$, where K is the Boltzmann constant, T is the absolute temperature of the photoacoustic cell. $\Delta Ev''$ is the vibrational energy in ground electronic state measured from $v'' = 0$, $A_{\rm nr}$ is the known radiative de-excitation probability and $h\nu$ is the energy of vibronic transition. The vibronic bands in the region 18480 to 19500 cm^{-1} involve excited state vibrational levels v' ranging from 21 to 43 as shown in figure 3a. The vibronic band frequencies of their relative photoacoustic

Table 1. Vibronic assignments of the photoacoustic spectra and the relative non-radiative decay rates between 18480 cm^{-1} and 19500 cm^{-1} of the $B \leftarrow X$ system of Br_2 molecules.

Observed band freq. (cm^{-1})	Relative photoacoustic intensity (I_{PA})	Assignment (v', v'')	Calculated band freq. (cm^{-1})	Calculated absorption intensity (I_{OA})	Relative non-radiative decay rate (A_{nr})
18489.0	0.28	(21,0)	18487.2	3.01	0.050
18571.0	0.76	(22,0)	18570.7	3.40	0.120
18607.7	1.11	(27,0)	18608.0	3.52	0.167
18651.5	1.44	(23,0)	18650.1	3.80	0.203
18668.6	1.48	(28.1)	18668.6	3.41	0.252
18724.6	0.87	(24,0)	18724.5	4.28	0.217
18724.6	0.87	(29,1)	18725.4	3.27	0.284
18778.8	1.70	(30,1)	18778.5	3.10	0.293
18801.0	1.78	(25,0)	28797.1	4.66	0.204
18876.0	1.84	(31,1)	18828.0	2.91	0.336
18867.0	2.06	(26,0)	18865.0	4.99	0.219
18875.0	2.04	(32,1)	18873.9	2.71	0.400
18915.8	2.04	(33,1)	18916.3	2.49	0.433
18929.0	2.14	(27,0)	18929.2	5.26	0.215
18992.0	2.12	(28,0)	18990.0	5.45	0.204
19047.2	2.18	(29,0)	19046.6	5.57	0.205
19100.0	2.22	(30,0)	19099.6	5.61	0.212
19149.9	2.30	(31,0)	19149.1	5.59	0.215
19196.0	2.36	(32,0)	19195.0	5.49	0.223
19236.8	2.38	(33,0)	19237.4	5.32	0.232
19278.6	2.41	(34,0)	19276.4	5.12	0.245
19309.0	2.44	(35,0)	19312.2	4.88	0.259
19345.0	2.50	(36,0)	19344.9	4.59	0.282
19371.9	2.54	(37,0)	19374.7	4.25	0.309
19401.2	2.56	(38,0)	19401.7	4.01	0.328
19425.6	2.58	(39,0)	19427.1	3.78	0.350
19450.1	2.60	(40,0)	19448.2	3.36	0.401
19468.0	2.63	(41,0)	19467.7	3.09	0.440
19487.0	2.65	(42,0)	19485.0	2.70	0.501
19501.2	2.70	(43,0)	19500.1	2.41	0.571

intensities and assignments are shown in the first, second and third columns of table 1 respectively. The frequencies of vibronic transitions were calculated from the vibrational constants reported by Coxan [1] and are given in column 4 of table 1. The absorption intensities of the vibronic bands were calculated from the Frank–Condon factors reported by Coxon [4] and these are included in column 5. The non-relative decay rates of relaxation from the excited vibronic levels are given in column six of table 1. The relative rate of non-radiative decay (see table 1) obtained from eq. (1) has been plotted in figure 4 and for comparison we have also plotted the radiative decay rate based on the work of Clyne and Heaven [7] which shows an inverse behaviour as expected. In the range of excited state vibrational quantum number $10 \leq v' \leq 50$ there are no abrupt changes in the non-radiative decay rate. This is in contrast to the case of the similar electronic transition of iodine molecule where the abrupt variation in non-radiative decay rate was explained as a result of predissociation from $23 \leq v' \leq 27$ in the B state [8].

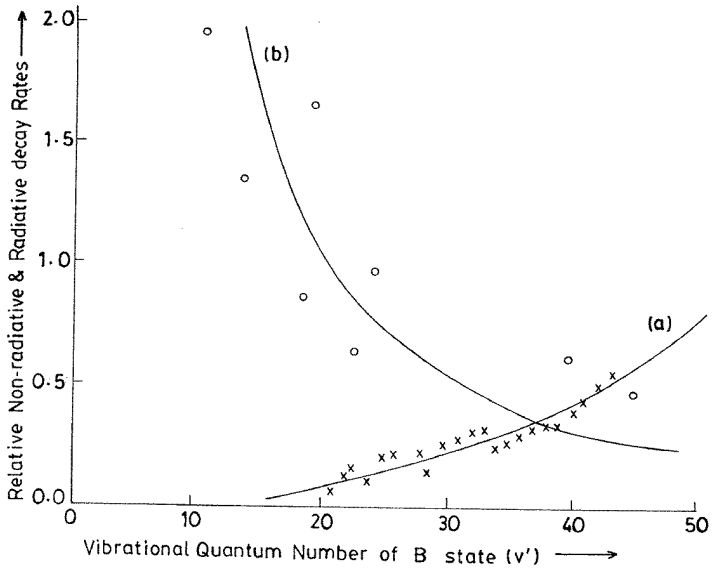

Figure 4. Variation of non-radiative (**a**) and radiative (**b**) decay rates with vibrational quantum numbers of $B^3\Pi^+_{0u}$ state.

5. Mechanisms of non-radiative decay in Br_2 vapour

The heat generation following excitation of the Br_2 molecules to the $B^3\Pi^+_{0u}$ state may result from the following processes:

(a) Vibrational-rotational relaxation in the $B^3\Pi^+_{0u}$ state.
(b) Predissociation of the $B^3\Pi^+_{0u}$ state mediated by the repulsive $^1\Pi$ state.
(c) Non-radiative de-excitation from the $B^3\Pi^+_{0u}$ state to the $X^1\Sigma^+_g$ state.
(d) Vibrational-rotational relaxation in the $X^1\Sigma^+_g$ state.

The heat energy released in processes (a) and (d) are generally a small fraction of the total optical energy absorbed by the molecule and the major heat signals are generated by non-radiative de-excitations (b) and (c). Clyne and Heaven [8] have concluded that the mean quantum yield of fluorescence using broad band excitation between 514 nm (18514 cm^{-1}) and 590 nm (16945 cm^{-1}) is less than 5%. This data suggests that about 95% of the excited Br_2 molecules relax non-radiatively. A large fraction of the discrete bands of the $B^3\Pi^+_{0u} \leftarrow X^1\Sigma^+_g$ absorption fall in this frequency range 18514–16945 cm^{-1} at 298 K. At the higher frequency end of this range the relative intensity of the background continuum is larger than that of the discrete bands whereas at 558 nm (17916 cm^{-1}) the ratio of the continuum to the discrete absorption considerably below unity is shown by Clyne and Heaven [7].

We have also used the absorption intensity measurements reported by Lindemann and Wiesenfeld [9] to estimate relative contributions of $B^3\Pi^+_{0u} \leftarrow X^1\Sigma^+_g$ and $^1\Pi \leftarrow X^1\Sigma^+_g$ transitions to the photoacoustic spectrum. These data have been normalized with

Table 2. Relative absorption strength of $B^3\Pi^+_{0u} \leftarrow X^1\Sigma^+_g$ and $^1\Pi \leftarrow X^1\Sigma^+_g$ transitions in the frequency range 17539–19994 cm^{-1}.

Wavelength (nm)	Frequency (cm^{-1})	$\in_{B\leftarrow X}$ (L. mol. cm^{-1})	$\in_{B\leftarrow X}(\lambda)$ / $\in_{B\leftarrow X(511\,nm)}$	$\in_{\Pi\leftarrow X}$ (L. mol. cm^{-1})	$\in_{\Pi\leftarrow X(\lambda)}$ / $\in_{\Pi\leftarrow X(511\,nm)}$
500	19994	62.1	1.57	11.50	2.06
505	19796	57.5	1.46	9.20	1.63
511	19579	49.0	1.25	7.00	1.25
520	19225	39.0	0.99	4.60	0.81
530	18862	29.9	0.76	2.87	0.51
535	18668	25.5	0.65	2.30	0.40
540	18514	20.7	0.50	–	–
550	18177	13.8	0.35	–	–
560	17852	7.0	0.19	–	–
570	17540	5.2	0.11	–	–

respect to absorption at 511 nm (19579 cm^{-1}) and are given in table 2. The relative intensities of $B^3\Pi^+_{0u} \leftarrow X^1\Sigma^+_g$ (figure 3b) and $^1\Pi \leftarrow X^1\Sigma^+_g$ (figure 3c) absorption have been adjusted to 1.25 at 511 (19579 cm^{-1}) so that these could be easily compared with the photoacoustic spectrum shown in figure 3a. It is found that the relative contribution of $^1\Pi \leftarrow X^1\Sigma^+_g$ absorption (figure 3c) exceeds that of $B^3\Pi^+_{0u} \leftarrow X^1\Sigma^+_g$ absorption (figure 3b) on the higher frequency side of the dissociation limit 511 nm. The absorption of $^1\Pi \leftarrow X^1\Sigma^+_g$ transitions is negligibly small on the lower frequency side of 18520 cm^{-1}. The sum of the relative intensities of figures 3b and 3c taken together account for the relative background in the photoacoustic spectrum shown in figure 3a. The increasing background continuum in figure 3a thus seems to result from the dominant role of $^1\Pi_{1u} \leftarrow X^1\Sigma^+_g$ non-radiative de-excitation. In addition to direct absorption $^1\Pi$ state the Br_2 molecules excited to the $B^3\Pi^+_{0u}$ state may also get transferred to the $^1\Pi_{1u}$ state from where they relax non-radiatively. There is indication of the $^1\Pi_{1u}$ and $B^3\Pi^+_{0u}$ potential curves touching each other at smaller values of inter-nuclear separations which may involve an easy predissociation of Br_2 molecules by transfer from the latter to the former as suggested by Tellinghuisen *et al* [10]. The presence of discrete bands of lower frequency side of 18520 cm^{-1} suggests that major contributions to photoacoustic signals comes from the direct non-radiative decay of Br_2 molecules from the $B^3\Pi^+_{0u}$ state to the ground state.

In view of the above discussion we reached the following conclusions regarding the mechanisms of non-radiative excitations of Br_2 molecules from the $B^3\Pi^+_{0u}$ state.

(a) For transition frequencies greater than 19579 cm^{-1} (511 nm), the photoacoustic signals result from dissociation of the $B^3\Pi^+_{0u}$ state with a larger contribution resulting from the dissociation of $^1\Pi_{1u}$ state.

(b) For transition in the frequency range 19579 cm^{-1} to 18520 cm^{-1} there is almost equal contribution to non-radiative decay of molecules from the $B^3\Pi^+_{0u}$ and the $^1\Pi_{1u}$ state as evidenced by figures 3b and 3c.

(c) For transitions with frequencies less than 18520 cm^{-1}, major part of the photoacoustic signal results from direct non-radiative decay of $B^3\Pi^+_{0u}$ state molecules to the ground state.

6. Conclusion

The non-radiative relaxation of the $B^3\Pi^+_{0u}$ state has been systematically investigated in the region of its dissociation limit by means of laser photoacoustic spectroscopy for the first time. The relative intensities of the banded and continuum spectra have been analysed in the light of earlier results of optical absorption and fluorescence spectroscopy of the $B^3\Pi^+_{0u} \leftarrow X^1\Sigma^+_g$ transitions. It is found that the background continuum results mainly due to photoacoustic signals from the repulsive $^1\Pi_{1u}$ state which overlaps with the $B^3\Pi^+_{0u}$ state. The banded structure in the photoacoustic spectrum comes from the non-radiative $B^3\Pi^+_{0u} \leftarrow X^1\Sigma^+_g$ de-excitation and the non-radiative rate constants determined from the relative intensities of these bands are found to increase as a function of increasing vibrational quantum number of the $B^3\Pi^+_{0u}$ state.

Acknowledgements

Partial financial support from a UGC-Volks Wagen sponsored research project on particle and photon spectroscopy of atoms and molecules is gratefully acknowledged.

References

[1] J A Coxon, *J. Mol. Spectrosc.* **37**, 39 (1971)
[2] J A Horsley and R F Barrow, *Trans. Faraday Soc.* **63**, 32 (1967)
[3] R F Barrow, T C Clark, J A Coxon and K K Yee, *J. Mol. Spectrosc.* **51**, 428 (1974)
[4] J A Coxon, *J. Quant. Spectrosc. Radiat. Trans.* **12**, 639 (1972)
[5] R J LeRoy, R G McDonald and G Burns. *J. Chem. Phys.* **65**, 1485 (1976)
[6] K Koseki, H Matsui and M Koshi, in *6th International Topical Meeting on Photoacoustic Photothermal Phenomena* (The Johans-Hopkins University, Baltimore Maryland, USA, July 31–August 3, 1989)
[7] M A A Clyne and M C Heaven, *J. Chem. Soc. Faraday Trans.* II **9**, 1992 (1978)
[8] K Narayanan and S N Thakur, *Appl. Opt.* **31**, 4987 (1992)
[9] T J Lindemann and J R Wiesenfeld, *J. Chem. Phys.* **70**, 2882 (1979)
[10] M A A Clyne, M C Heaven and J Tellinghuisen, *J. Chem. Phys.* **76**, 5341 (1982)